

# UCSF

## UC San Francisco Previously Published Works

### Title

Inhibitor Combinations Reveal Wiring of the Proteostasis Network in Prostate Cancer Cells

### Permalink

<https://escholarship.org/uc/item/0md990s0>

### Journal

Journal of Medicinal Chemistry, 64(19)

### ISSN

0022-2623

### Authors

Shkedi, Arielle  
Adkisson, Michael  
Schroeder, Andrew  
[et al.](#)

### Publication Date

2021-10-14

### DOI

10.1021/acs.jmedchem.1c01342

Peer reviewed



Published in final edited form as:

*J Med Chem.* 2021 October 14; 64(19): 14809–14821. doi:10.1021/acs.jmedchem.1c01342.

## Inhibitor Combinations Reveal Wiring of the Proteostasis Network in Prostate Cancer Cells

Arielle Shkedi<sup>1</sup>, Michael Adkisson<sup>2</sup>, Andrew Schroeder<sup>2</sup>, Walter L Eckalbar<sup>2</sup>, Szu-Yu Kuo<sup>1</sup>, Leonard Neckers<sup>3</sup>, Jason E. Gestwicki<sup>1,\*</sup>

<sup>1</sup>Department of Pharmaceutical Chemistry and the Institute for Neurodegenerative Disease, University of California San Francisco, San Francisco CA 94158

<sup>2</sup>Functional Genomics Core, University of California San Francisco, San Francisco, CA 94158

<sup>3</sup>Urologic Oncology Branch, Center for Cancer Research, National Cancer Institute, Bethesda, MD 20892

### Abstract

The protein homeostasis (proteostasis) network is composed of multiple pathways that work together to balance protein folding, stability and turnover. Cancer cells are particularly reliant on this network; however, it is hypothesized that inhibition of one node might lead to compensation. To better understand these connections, we dosed 22Rv1 prostate cancer cells with inhibitors of four proteostasis targets (Hsp70, Hsp90, proteasome and p97), either alone or in binary combinations, and measured effects on cell growth. The results reveal a series of additive, synergistic and antagonistic relationships, including strong synergy between inhibitors of p97 and the proteasome, and striking antagonism between inhibitors of Hsp90 and the proteasome. Based on RNA-seq, these relationships are associated, in part, with activation of stress pathways. Together, these results suggest that cocktails of proteostasis inhibitors might be a powerful way of treating some cancers, although antagonism that blunts the efficacy of both molecules is also possible.

### Keywords

heat shock protein; Hsp70; Hsp90; chaperones; proteasome; 26S; VCP; p97; prostate cancer; androgen receptor; synergy

### Introduction

The proteostasis network is a highly conserved set of pathways that balances the synthesis, folding, activation, and degradation of the proteome<sup>1</sup>. There are hundreds of components dedicated to this network, including molecular chaperones (*e.g.* heat shock proteins),

\*Correspondence can be addressed to: Jason E. Gestwicki, Ph.D., UCSF, 675 Nelson Rising Lane, San Francisco, CA 94158, Phone: 415-502-7121, jason.gestwicki@ucsf.edu.

**Supporting Information.** Supporting information is included, which contains Figures S1–S4.

**Conflict of Interest Disclosure.** J.E.G. is an inventor on patents associated with Hsp70 inhibitors and their use in cancer.

co-chaperones, the translation machinery, the ubiquitin-proteasome system and autophagy-lysosome pathway<sup>2, 3</sup>. This network is characterized by major “nodes” that are connected, often through direct protein-protein interactions, with the other components<sup>4</sup>. Importantly, the flux of proteins through this network is tightly regulated by stress signaling, including the unfolded protein response (UPR), the integrated stress response (ISR), the heat shock response (HSR) and others<sup>5-8</sup>. Specifically, stress signaling often elevates the levels of proteostasis factors, such as some chaperones, as well as tuning the rates of protein synthesis and turnover, allowing cells to adapt to changing conditions. Thus, the proteostasis network is both interconnected and responsive, likely allowing different sub-networks to play dominant roles in response to specific perturbations<sup>9</sup>.

Cancer cells have been found to be particularly reliant on specific components of the proteostasis network, likely because of the rapid growth, high frequency of translation errors and genomic instability of these cells<sup>10, 11</sup>. For example, major nodes of the proteostasis network, such as Hsp70, Hsp90 and HSF1, are important for maintaining tumorigenesis<sup>7, 12, 13</sup>. In contrast, normal, untransformed cells seem to be less reliant on these same proteostasis factors, perhaps because their networks are more robust to the loss of an individual component. The mechanistic reasons for differential vulnerability are often not clear, but recent studies have started to provide insights. For example, Hsp90 binds to a distinct set of co-chaperones in cancer cells vs. non-transformed cells<sup>14,15</sup>, suggesting that the same node can be “wired” differently following tumorigenesis.

These observations, and others, have led to the hypothesis that nodes of the proteostasis network are promising drug targets, which could be exploited for anti-cancer therapy<sup>16-19</sup>. Accordingly, substantial efforts have been mobilized to create chemical inhibitors of proteostasis targets<sup>20-22</sup>. Although this remains an active research area, a subset of these molecules has advanced to the clinical setting, with varying levels of success. For example, proteasome inhibitors are approved and widely used in treating multiple myeloma<sup>23</sup>. However, inhibitors of other proteostasis targets have been less successful<sup>24-26</sup>, often due to lack of efficacy, rapid onset of resistance and/or unacceptable toxicity. Moreover, even proteasome inhibitors are ineffective at treating some cancer subtypes, such as solid tumors, for reasons that remain uncertain<sup>27</sup>.

One hypothesis to explain the uneven and sometimes confounding clinical results is that the interconnected nature of the proteostasis network might create opportunities for compensation by stress responses<sup>28</sup>. For example, it is well established that treatment with Hsp90 inhibitors, at least those that bind the N-terminal domain, leads to elevated expression of Hsp70 and other chaperones via an HSR program<sup>10</sup>. Similarly, proteasome inhibitors induce autophagy pathways<sup>29</sup>, and inhibition of p97 activates the UPR<sup>22</sup>. Mounting evidence suggests that these compound-induced, stress responses might directly contribute to inhibitor resistance. For example, activation of autophagy and other stress pathways<sup>28</sup> makes certain cancer cells relatively resistant to Hsp70 inhibition<sup>30</sup>. Additionally, activation of the HSR has been linked to bortezomib resistance in multiple myeloma<sup>31,32</sup>. Thus, cancer cells seem to activate stress pathways in response to proteostasis inhibitors, which can, in some cases, provide them with partial protection.

Because the nodes of the proteostasis network are inter-connected and subject to regulation by stress responses, combinations of proteostasis inhibitors might, in some cases, be strongly synergistic<sup>33</sup>. Specifically, inhibition of two proteostasis targets simultaneously might limit the ability of cancer cells to circumvent loss of one target. However, while some promising combinations have been proposed<sup>34–36</sup>, this possibility has not been systematically explored. Here, we tested four proteostasis inhibitors by themselves and in binary combinations to reveal additive, synergistic and antagonistic relationships. We chose to perform these screens in 22Rv1 prostate cancer cells, given the known reliance of these cells on the proteostasis network<sup>37, 38</sup>. As test compounds, we selected four well-known inhibitors that target major nodes in the proteostasis network: Hsp70, Hsp90, the 26S proteasome and VCP/p97. Briefly, Hsp70 and Hsp90 are molecular chaperones involved in protein folding and activation<sup>39</sup>. VCP/p97 is a AAA<sup>+</sup> ATPase which plays multiple roles in protein trafficking and quality control<sup>40</sup>, and the 26S proteasome is responsible for degrading ubiquitinated proteins<sup>41</sup>. Beyond their individual functions, these nodes also engage in functional relationships within a defined sub-network (Figure 1A). For example, Hsp70 delivers unfolded proteins to Hsp90 through a shared co-chaperone, Hop<sup>42, 43</sup>. Moreover, p97 collaborates with Hsp70 and the proteasome during ER-associated degradation (ERAD)<sup>44, 45</sup> and both Hsp70 and Hsp90 are involved in delivering proteins to the proteasome for degradation<sup>46, 47</sup>. Thus, we were interested in whether an inhibitor of one node in this particular sub-network might create synergy with inhibitors of others.

To target these four nodes, we selected well-characterized chemical inhibitors: JG-98 (Hsp70 inhibitor)<sup>48</sup>, 17-DMAG (Hsp90 inhibitor)<sup>49</sup>, bortezomib (proteasome inhibitor)<sup>50</sup> and CB-5083 (p97 inhibitor)<sup>22</sup> (Figure 1B). These compounds were selected because three of them have been explored in clinical trials, while the fourth, JG-98, is a close analog of a molecule, MKT-077, tested in Phase I<sup>51</sup>. Using a high throughput, 384-well growth assay, we tested binary combinations of the compounds on growth of 22Rv1 prostate cancer cells, revealing examples of both synergy (Hsp70-Hsp90, p97-Hsp90, p97-proteasome) and antagonism (Hsp70-proteasome, Hsp90-proteasome). Transcriptome studies on cells treated with the most promising combinations revealed differences in the cellular stress response(s) compared to the single agent treatments, perhaps underlying, in part, the observed relationships. Also, repeating these screens in three additional prostate cancer cell lines, C4-2, LNCaP and PC3, identified both shared and cell-type specific relationships, suggesting that the “wiring” of the proteostasis network can partially differ across cell lines. Together, these studies show that testing proteostasis inhibitor combinations in cultured cells reveals patterns of additivity, synergy and antagonism, which could aid in the design (or avoidance) of therapeutic combinations for use in the clinic.

## Results

### **Proteostasis inhibitors reduce cell viability in 22Rv1 prostate cancer cells, as single agents.**

To provide a baseline for combination studies, we first confirmed the effects of the four proteostasis inhibitors: JG-98 (Hsp70 inhibitor), 17-DMAG (Hsp90 inhibitor), bortezomib (proteasome inhibitor) and CB-5083 (p97 inhibitor) on growth of 22Rv1 cells as single

agents. After a 72-hour treatment, each of the inhibitors, but not the DMSO control, reduced growth of 22Rv1 cells, with  $IC_{50}$  values varying from 0.02 to 3.3  $\mu$ M (Figure 1B). Consistent with observations from the literature, inhibitors of Hsp70, p97, and the proteasome reduced cell viability to nearly baseline at the highest doses, while Hsp90 inhibition produced a ~50% reduction, even at the highest concentrations.

### Combination treatments reveal patterns of additivity, synergy and antagonism upon proteostasis disruption.

Based on the calculated  $IC_{50}$  values, we then chose compound concentration ranges for use in the combination screens (see Methods). First, 22Rv1 cells were plated in 384-well plates, and, on the following day, compounds were added using standard laboratory automation. Treatments were performed in quadruplicate (4 wells per treatment) and each compound was tested in 8 concentrations (DMSO control, plus 7 doses in 2-fold dilutions; Figure 2). After 3 days of treatment, cell viability was quantified using Cell Titer Glo. From the resulting data, all of the values in the 8x8 treatment matrix were used to calculate synergy values using the ZIP synergy model<sup>52</sup> (Figure 2). There are multiple methods for estimating potential synergy or antagonism between compounds<sup>53, 54</sup> and consensus in which approach to select has been elusive<sup>55, 56</sup>. In this case, we chose to use ZIP synergy because it utilizes the entire dose-response landscape (Figure 2, Figure S1), ensuring that all of the doses are represented when determining the numerical synergy value. This feature was especially important here because the Hsp90 inhibitor 17-DMAG did not reduce viability to baseline, which we found could create misleading synergy values if other approaches were employed. In this study, we considered scores to be additive if they were between the values of +1.5 and -1.5, while scores greater than +1.5 were categorized as synergistic and those less than -1.5 were antagonistic. We arrived at these arbitrary cutoff values by comparing the variance of the ZIP synergy scores across replicates and by manually examining the dose-response curves (see below). Importantly, this protocol and analysis pipeline was reproducible, with independent replicates on different days showing high correlation (Figure S1).

From the combination screens in 22Rv1 cells, we observed clear patterns of additivity, synergy and antagonism between the proteostasis inhibitors. For example, the combination of Hsp70 and p97 inhibitors was additive (ZIP score ~ 1.2), as co-treatment with the p97 inhibitor did not significantly impact the apparent  $IC_{50}$  of the Hsp70 inhibitor (Figure 3). However, other combinations, such as Hsp90-p97, Hsp90-Hsp70 and proteasome-p97, were found to be synergistic. The combinations of Hsp90-p97 and Hsp70-Hsp90 were modestly synergistic (ZIP scores between +2.4 and +2.8), while the combination of p97 and proteasome inhibitor (compounds bortezomib and CB-5083) was the most strongly synergistic, with a ZIP score of +9.1. This relationship is illustrated by examining a subset of the dose response curves, in which bortezomib alone is able to decrease cell viability (Figure 3; black curve), but the apparent  $IC_{50}$  is enhanced when CB-5083 is added (Figure 3; blue curves). These findings of strong synergy confirm the long-standing idea that targeting two proteostasis nodes might, in some cases, enhance cancer cell death.

In addition to synergistic combinations, we were surprised to observe combinations that were antagonistic. For example, the Hsp70-proteasome combination was moderately

antagonistic (ZIP score  $-5.5$ ). This effect seemed most prominent at the higher doses of Hsp70 inhibitor, as is clear from examination of a subset of dose-response curves that show that the proteasome inhibitor (Figure 3; black curves) becomes less effective when the cells are also dosed with an Hsp70 inhibitor (Figure 3; blue curves). More strikingly, we found that the combination of Hsp90 and proteasome inhibitors was strongly antagonistic (ZIP score  $-19.9$ ). In a representative series of results, addition of 17-DMAG (Figure 3; blue curves) clearly suppresses the anti-proliferative activity of bortezomib compared to this compound alone (Figure 3; black curve). Indeed, at the higher doses of the Hsp90 inhibitor, the anti-proliferative effects of the proteasome inhibitor are nearly abolished. Thus, some proteostasis combinations can be strongly antagonistic.

To provide additional insight, we repeated a subset of the combination treatments, replacing 17-DMAG for an alternative Hsp90 inhibitor, AUY-922. In those studies, we observed effects consistent with those obtained using 17-DMAG (Figure S2A), suggesting that anti-proliferative activities are, at least in part, a product of target biology and not specific to the compound. Next, we repeated the screens using a non-tumorigenic prostate cell line RWPE-1 and found no strong synergy between any drug combination (Figure S2B). Thus, the combinations did not seem to generally increase toxicity to cells, but rather, to enhance selectivity for 22Rv1 cancer cells over the non-tumorigenic cells. Finally, we wanted to ensure that the handling steps do not contribute to the observed synergy values, so we repeated the combinations by testing compounds against themselves. In those studies, we found no synergy or antagonism (Figure S2C), giving additional confidence in the screening platform.

#### **Androgen receptor (AR) stability may explain some, but not all, drug synergies.**

We next wanted to explore possible mechanisms of synergy and/or antagonism. 22Rv1 cells are a prostate cancer cell line that is reliant on androgen receptor (AR) signaling<sup>57</sup>. However, these cells are relatively resistant to anti-androgen therapy because they express both full length (FL) AR and androgen-independent splicing variants (ARv) associated with severe disease<sup>58</sup>. AR and its variants are established clients of Hsp70 and Hsp90<sup>37</sup> and inhibitors of these chaperones have been shown to promote degradation of AR and ARv<sup>37, 59</sup>. Indeed, we confirmed that treatment with combinations of JG-98 and 17-DMAG leads to loss of FL and ARv in 22Rv1 cells (Figure 4A), reducing AR to  $\sim 10\%$  of total and ARv to  $\sim 60\%$  of total. Consistent with previous reports<sup>37</sup>, the single agent treatments show that Hsp70 inhibition has a more dramatic effect on ARv, while Hsp90 inhibition preferentially destabilizes FL AR. Thus, Hsp70 and Hsp90 inhibitors may be synergistic because their co-treatment leads to lower levels of both AR and ARv, interrupting the AR signaling required for growth of these cells. However, AR stability did not explain all of the synergies. For example, treatment with the synergistic combination, p97-proteasome, did not alter either AR or ARv levels under the same conditions (Figure 4B). Likewise, AR stability did not correlate with synergy or antagonism after co-treatment with inhibitors of p97-Hsp70, Hsp70-proteasome, or Hsp90-proteasome (Figure S3), as there was no substantial differences between single-agents and combination treatments. Together, these results suggest that AR stability can be important, but that different mechanism(s) may be underlying drug synergy and antagonism in response to most of the combinations.

### **RNASeq experiments reveal differential activation of stress responses that occur after treatment with inhibitor combinations.**

To examine the downstream effects of proteostasis inhibition in an unbiased way, RNA-seq was used to identify transcriptional differences in the response of 22Rv1 cells to compounds and their combinations. Based on the growth assays, we focused these studies on 9 treatment conditions: a DMSO control, Hsp70, Hsp90, p97, or proteasome inhibition alone, and the Hsp70-Hsp90, p97-proteasome, and Hsp90-proteasome combinations. These combinations were selected to sample both synergistic (Hsp70-Hsp90 and p97-proteasome) and antagonistic (Hsp90-proteasome) examples. In the RNA-Seq studies, compounds were tested at a single concentration, selected by considering both the IC<sub>50</sub> values (see Figure 1) and the results from the ZIP synergy analysis (see Methods).

22Rv1 cells were treated for 6 hours with the indicated compounds in triplicate, after which RNA was extracted and RNA-seq was performed (see Methods). Read count data was analyzed by DeSeq2 and the top 100 variably expressed genes were hierarchically clustered and visualized (Figure 5). First, we noted that almost all of the biological replicates clustered together, suggesting a reproducible and specific transcriptional response to each treatment. The only outlier was the combination of JG-98 (Hsp70 inhibitor) and 17-DMAG (Hsp90 inhibitor), where one of the three replicates did not immediately co-cluster. Next, we further subdivided the top 100 variably expressed genes across all the treatments into 5 clusters (Cluster 1-5) and examined them via gene ontology (GO) analysis (Figure 6A). Cluster 1 contains stress response genes, such as DDIT4 and SESN2, as well as ER stress response genes linked to the UPR, including HSPA5 (BiP, an ER Hsp70) and DDIT3 (CHOP). Cluster 2 contains many heat shock proteins and co-chaperones, including multiple Hsp70s (HSPA1B, HSPA1A, HSPB1, HSPH1, HSPA8), Hsp90s (HSP9-AA1, HSP90AB1), Hsp70 co-chaperones (DNAJA1 and BAG3), and ubiquitin (UBB). These genes are known to be upregulated following Hsp90 inhibition, but we additionally found that this effect is exacerbated by the combined Hsp90-proteasome inhibition (Figure 5). Qualitatively, this group of genes includes many hallmarks of the HSR<sup>60</sup>. Clusters 3 and 5 produced less well-defined GO terms, and their relevance will require additional study. However, we were interested to find that Cluster 4 contains exclusively mitochondrially expressed genes (Figure 5). The mitochondrial genome contains 37 genes, and we observed up-regulation of a significant portion following treatment with either JG-98 alone or the JG-98 and 17-DMAG combination. JG-98 has been shown to target mitochondrial Hsp70<sup>48, 61</sup>, and it seems likely that, in these cells, it impacts mitochondrial proteostasis.

### **Immunoblotting validates the RNA-seq results and highlights differences in stress responses caused by proteostasis inhibition.**

To validate a subset of these RNA-Seq findings, we examined the protein levels of representative stress response effectors, BiP (marker of the UPR) and Hsp72 (marker of the HSR), following proteostasis inhibition in the treated 22Rv1 cells (Figure 6C). We also monitored the levels of Hsc70/HSPA8, which is typically more mildly upregulated in the HSR. After 24 hours of compound treatment, we observe BiP upregulation following inhibition of the proteasome or p97 and after treatment with the p97 inhibitor or the combinations of p97-proteasome or Hsp90-proteasome inhibitors, which is consistent with

the RNASeq results. In multiple myeloma cells, inhibitors of p97 have also been shown to activate the UPR, leading to elevated BiP levels<sup>22</sup>. Additionally, we observed that Hsp72 is elevated following treatment with either the Hsp90 inhibitor, the proteasome inhibitor or the Hsp90-proteasome inhibitor combination in 22Rv1 cells (Figure 6C). Interestingly, the response to the combination was generally stronger than Hsp90 or proteasome inhibition alone, consistent with the RNA-Seq results. Thus, we hypothesized that one mechanism driving antagonism between Hsp90 and proteasome inhibitors may be the strong upregulation of HSR genes, which might blunt the activity of both compounds. To test this idea, we combined proteasome inhibitor treatment with heat stress instead of the Hsp90 inhibitor. This experiment was designed to discern whether the antagonism was due to the effects of Hsp90 inhibitor on the HSR or its ability to destabilize the chaperone's clients.<sup>62, 63</sup> Accordingly, 22Rv1 cells were placed at 42 °C for either 15, 30 or 120 minutes and then treated with bortezomib. One important caveat in this experiment is that we were unable to maintain heat shock during the entire 72 hr growth phase that is required for bortezomib-mediated anti-proliferative activity. However, even with this caveat, it was still striking that the potency of bortezomib was unchanged by any of the heat shock treatments (Figure S4). Thus, the antagonism between inhibitors of Hsp90 and the proteasome might potentially involve destabilization of Hsp90 clients.

#### **Additional prostate cancer cell lines have both similar and distinct patterns of sensitivity to proteostasis inhibitors.**

Lastly, we probed how these patterns of drug synergy/antagonism might compare across other prostate cancer cell lines. For these studies, we chose three cell lines: LNCaP, C4-2, and PC-3. Briefly, LNCaP cells are an androgen-sensitive prostate cell line, and C4-2 cells are an androgen insensitive cell line derived from LNCaP. Like 22Rv1 cells, both LNCaP and C4-2 express AR and are driven by AR signaling, while PC-3 cells are a prostate line that are androgen-insensitive and do not express AR. Thus, we expected that screens in these cell lines could reveal potential synergies across a wider range of prostate cancer cell types with different origins, AR status, and anti-androgen sensitivities.

We treated the three cell lines with an 8x8 matrix of compounds and summarized the resulting additivity, synergy and antagonism through calculation of ZIP synergy scores. In Figure 7, we also include the results from the 22Rv1 cell lines (see Figure 3) again for clarity and comparison. Together, the results revealed that there are some similarities across the prostate cancer cell lines, but that none of them respond exactly the same way (Figure 7A). Among the similarities, the combination of Hsp70-p97 inhibitors tended to be synergistic (ZIP values between +1.2 to 3.2) and the combination of Hsp90-proteasome inhibitors was always antagonistic (ZIP synergy values between -6.9 and -19.9). The shared, antagonistic response to combinations of Hsp90 and proteasome inhibitors was especially intriguing. Examination of the dose response curves from this series confirmed that proteasome inhibitor (bortezomib) was toxic to all the cells, but that addition of Hsp90 inhibitor (17-DMAG) could make the compound less effective (Figure 7B), although this effect was more modest in the PC-3 cells. To explore whether this antagonism might be linked to up-regulation of Hsp72, we performed western blots on the treated lysates. As we observed in the 22Rv1 cells, addition of an Hsp90 inhibitor to the proteasome inhibitor

strongly up-regulates Hsp72 at 24 hours in each cell line (Figure 7C) and the level of elevation was greater than with either compound alone. There are hundreds of known Hsp90 clients,<sup>62, 63</sup> we have not yet been able to explore whether destabilization of these might be linked to antagonism across the four cell lines.

In addition to these similarities across the four cell lines, we also noted that some relationships depend on the cell type. For example, the combination of Hsp70-Hsp90 inhibitors was only synergistic (ZIP score +2.4) in the 22Rv1 cells (Figure 7A) and was generally antagonistic in the other cell lines (ZIP score between -4.4 and -4.9). 22Rv1 cells are the only line tested here that expresses both AR and ARv, so this could be one contributing factor (see Figure 3). Indeed, ARv has been shown to drive both overlapping and unique transcriptional programs, compared to AR<sup>64</sup>; thus, loss of both factors might be especially required in 22Rv1 cells. Together, these results highlight the importance of characterizing the wiring of the proteostasis network in each cell line or tumor model because the exact pattern of synergy/antagonism can depend on the cell line.

## Discussion

The proteostasis network holds great promise as a source of drug targets for anti-cancer treatment<sup>9, 65</sup>. However, this concept has met with both successes and failures in the clinic, perhaps requiring a re-examination of the treatment strategies. One logical approach is to use inhibitor combinations, which might limit the ability of cancer proteostasis networks to compensate for loss of one pathway. Although it had been hypothesized that combinations of proteostasis inhibitors might have additivity or even synergy in cancer cells, this possibility had not been systematically quantified. Using a high throughput platform, we revealed clear and reproducible patterns of additivity, synergy and antagonism between inhibitors of four major proteostasis nodes in four different prostate cancer cell lines. We observed that p97 and proteasome inhibitors were especially synergistic in 22Rv1 cells (ZIP score 9.1), a model of castration-resistant prostate cancer (CRPC). Thus, this combination might be used to reduce the dose required for both compounds, potentially improving potency while reducing toxicity. In support of this idea, the p97-proteasome inhibitor combination did not produce enhanced cell growth inhibition in non-tumorigenic RWPE-1 cells (see Figure S2B). However, it is also important to note that synergy for this combination was not observed in the other three prostate cancer lines, where this combination was modestly antagonistic. Thus, a tailored therapeutic strategy might be required, such as screening primary cells against combinations *ex vivo* to identify synergistic relationships. Future work will be required to understand whether expression and stability of AR and ARv (see Figure 4A) is predictive of this synergy, as the 22Rv1 cells are the only line tested that expresses both.

We were initially surprised to find drug combinations, exemplified by the Hsp90 and proteasome inhibitor pair, that showed striking antagonism. Within the chosen subnetwork (see Figure 1A), we initially hypothesized that synergy might predominate because of the collaboration between these factors. However, recent studies have introduced the idea of “single-agent dominance” in two-drug combinations<sup>66</sup>. In this paradigm, molecules that produce a faster onset of cell death can dominate the co-treatment because of cross-

talk between cell death pathways. Inhibition of Hsp70, for example, has been shown to rapidly induce both apoptosis and necroptosis<sup>67</sup>, so a deeper exploration of the role of cell death pathways and their kinetics will need to be explored for proteostasis inhibitors. Another possibility, potentially supported by our RNA-Seq and western blot findings and not mutually exclusive of “single-agent dominance”, is that the stress responses might be partially responsible for the relationships between compound treatments. For example, the prostate cancer cells might activate the HSR to compensate for loss of function of either Hsp90 or the proteasome. In support of this idea, the combination produces a more robust HSR activation (see Figure 7C). However, the combination of heat shock with proteasome inhibitor was not antagonistic (see Figure S4), suggesting that other factors, such as destabilization of Hsp90 client proteins, might also play an important role. Hsp90 regulates the stability of hundreds of client proteins<sup>62, 63</sup>, and it remains to be seen which ones might be involved in antagonism. Regardless, some evidence suggests that the relationship between Hsp90 and proteasome inhibitors might also depend on the type of cancers. For example, in multiple myeloma cells, treatment with a combinations of Hsp90 and proteasome inhibitors has been suggested to be potentially synergistic based on pre-clinical studies<sup>68, 69</sup> and a clinical trial was conducted in multiple myeloma patients.<sup>69, 70</sup> While our studies were in prostate cancer cells, and not multiple myeloma, it seems possible that stratifying patients based on induction of the HSR and/or destabilization of Hsp90 clients might have helped parse the most likely to respond favorably.

Together, these results suggest that a more comprehensive understanding of which stress pathways are activated by proteostasis inhibitors is likely needed to better track and, ultimately, predict synergy/antagonism, with the goal of designing more effective treatment strategies. One major goal of those efforts could be to profile which stress response pathways, such as HSR, UPR, autophagy, *etc.* are activated by inhibitors, so that predictive biomarkers could be identified<sup>71, 72</sup>. Moreover, a deeper understanding of which Hsp90 clients are de-stabilized by inhibitors in specific cell types is lacking. Finally, it is starting to become clear that this framework could be more broadly important outside proteostasis targets, as well. For example, treatment with other chemotherapeutics and radiation are capable of eliciting stress responses<sup>73, 74</sup>, which might likewise blunt their efficacy. Thus, clinical biomarkers of stress responses might have important impacts outside programs associated with proteostasis targets.

## Experimental

### Cell lines.

22Rv1, LNCaP, C4-2, and PC-3 cells were purchased from ATCC and grown in RPMI 1640 medium supplemented with 10% non heat-inactivated FBS (Gibco 16000044) and 1% penicillin/streptomycin. RWPE-1 cells were purchased from ATCC and grown in K-SFM supplemented with bovine pituitary extract and human recombinant EGF. All cells were grown at 37 °C and 5% CO<sub>2</sub>. Cells were regularly tested for mycobacterial contamination (every 6 months), and maintained at a low passage number.

### Inhibitors.

JG-98 was prepared, as described<sup>48</sup>, and determined to be >95% pure by HPLC. 17-DMAG was purchased from Cayman Chemical (item #11036). CB-5083 was purchased from Fisher Scientific (catalog #50-115-2549). Bortezomib was purchased from Millipore Sigma (CAS 179324-69-7). AUY-922 was purchased from Fisher Scientific (CAS #747412-49-3). Commercial compounds are reported by the manufacturer to be 95% pure by HPLC.

### Drug combinations and synergy.

All tested compounds were prepared as 10 mM stocks in DMSO and stored in aliquots at  $-20^{\circ}\text{C}$ . For treatments, compounds were then serially diluted in 2-fold increments in RPMI (final DMSO  $\sim 0.02\%$ ). These solutions were then aliquoted to 96-well plates in an 8x8 matrix format for each combination. Concentrations were chosen based on the  $\text{EC}_{50}$  value of each compound in the cell lines tested, to center the dilution series on the half-maximal value. Specifically, the following final concentrations were used: JG-98 (0.16 to 10  $\mu\text{M}$ ), 17-DMAG (0.016 to 1  $\mu\text{M}$ ), CB-5083 (0.078 to 5  $\mu\text{M}$ ), bortezomib (0.0015 to 0.1  $\mu\text{M}$ ). Each compound was tested in 7 doses (plus a DMSO solvent control), using 2-fold serial dilutions.

Cells were grown in tissue-culture treated, 384-well plates (Corning). After 24 hours of cell growth, an Agilent robot was used to transfer compound from the 96-well plates to these 384-well test plates. Cells were returned to  $37^{\circ}\text{C}$  and 5%  $\text{CO}_2$  and grown for three days (doubling time 30-50 hours depending on the cell line). Cell viability was measured using Cell Titer Glo (Promega) according to the manufacturer's instructions and luminescence was measured with a SpectraMax M5 plate reader (Molecular Devices). Cell viability was normalized per plate to the untreated, DMSO control. Synergy was determined using SynergyFinger (<http://www.synergyfinderplus.org/>). All drug combinations were performed twice per cell line (in technical quadruplicates), and the average mean synergy score for the entire dataset was reported.

### Immunoblotting.

Cells were plated in 6-well or 12-well plates at 80-100% confluency for 24 hours, after which the medium was replaced with fresh medium containing indicated compounds at 1% DMSO. Compounds were left on cells for the indicated time period (6-24 hours), and cells were incubated at  $37^{\circ}\text{C}$  and 5%  $\text{CO}_2$ . Cell lysate was then harvested with M-PER supplemented with protease inhibitor. For measuring phospho-proteins, M-PER was additionally supplemented with phosphatase inhibitor. Lysate was then run on 4-15% gradient SDS polyacrylamide gels at 5-10  $\mu\text{g}$  of total protein per sample. Proteins levels were detected either with Licor florescent secondary antibodies and detected with a Licor machine, or HRP-conjugated secondary antibodies and imaged with BioRad. The following antibodies were used:

### Antibodies

The following antibodies were used for immunoblotting: AR (Abcam #ab133273, 1:2000, rabbit), BiP (CST #3177, 1:2000, rabbit), Hsc70/HSPA8 (Enzo ADI-SPA-816-F, 1:2000,

rabbit), Hsp72/HSPA1A (Enzo ADI-SPA-811-F, 1:2000, rabbit) and actin (Sigma A2228, 1:5000, mouse).

## RNAseq and Western blot validation

Treatment concentrations were chosen based on dose-response and drug synergy data, to best capture combinations of compounds that were either synergistic or antagonistic. Specifically, the following concentrations were used: JG-98 (0.625  $\mu$ M), 17-DMAG (0.25  $\mu$ M), CB-5083 (0.625  $\mu$ M) and bortezomib (0.025  $\mu$ M). For RNA-seq studies, 22Rv1 cells were plated at 80% confluency in 12-well plates. After 24 hours, cells were dosed with compounds at indicated concentrations and incubated at 37 °C and 5% CO<sub>2</sub>. After 6-hour treatment, RNA was extracted using Zymo Quick-RNA miniprep kit (Catalog #R1054). RNA from all samples were diluted to 20ng/uL in 10 uL for input into TECAN Universal plus mRNA-seq library preparation. RNA-seq libraries were prepared using the manufacture's protocol. RNA-seq libraries were sequenced for quality control on an Illumina MiniSeq and pooled according to protein coding read counts to obtain uniform protein coding read depth. The final pools were sequenced using single end 50bp reads on an Illumina HiSeq 4000 at the Center for Advanced Technology ([www.cat.ucsf.edu](http://www.cat.ucsf.edu)). Sequencing reads were aligned to the Human reference genome (Build HG38) and the Ensembl gene annotation (version 95) using STAR (v2.7.2b; PMID: 23104886). Read counts per gene as output by STAR were collapsed into a read counts matrix and were used as input to DESeq2 (v1.24.0; PMID: 25516281) to test for differential gene expression between conditions using a Wald test. Genes passing a multiple testing correct p-value of 0.1 (FDR method) were considered significant. For western blot validation of RNA-seq, 22Rv1 cells were plated and dosed at the same conditions. Following drug-treatment, immunoblotting was performed as described above.

## Supplementary Material

Refer to Web version on PubMed Central for supplementary material.

## Acknowledgements.

This work was supported by grants from the US Department of Defense (PC180716 and PC150065; to J.E.G. and L.N.), the NIH (NS059690 to J.E.G.) and the Mary A. Koda-Kimble Seed Award (to A.S.). The authors additionally thank S. Sannino and J. Brodsky (U. Pittsburgh) and A. Witta (UCSF) for helpful comments and advice.

## Abbreviations Used.

<b>AR</b>	androgen receptor
<b>ARv</b>	androgen receptor variant
<b>17-DMAG</b>	17-Dimethylaminoethylamino-17-demethoxygeldanamycin
<b>ERAD</b>	ER-associated degradation
<b>ISR</b>	integrated stress response
<b>Hop</b>	Hsp70-organizing protein

<b>HSF1</b>	heat shock factor 1
<b>Hsp70</b>	heat shock protein 70
<b>Hsp90</b>	heat shock protein 90
<b>HSR</b>	heat shock response
<b>UPR</b>	unfolded protein response
<b>VCP</b>	valosin-containing protein

## References

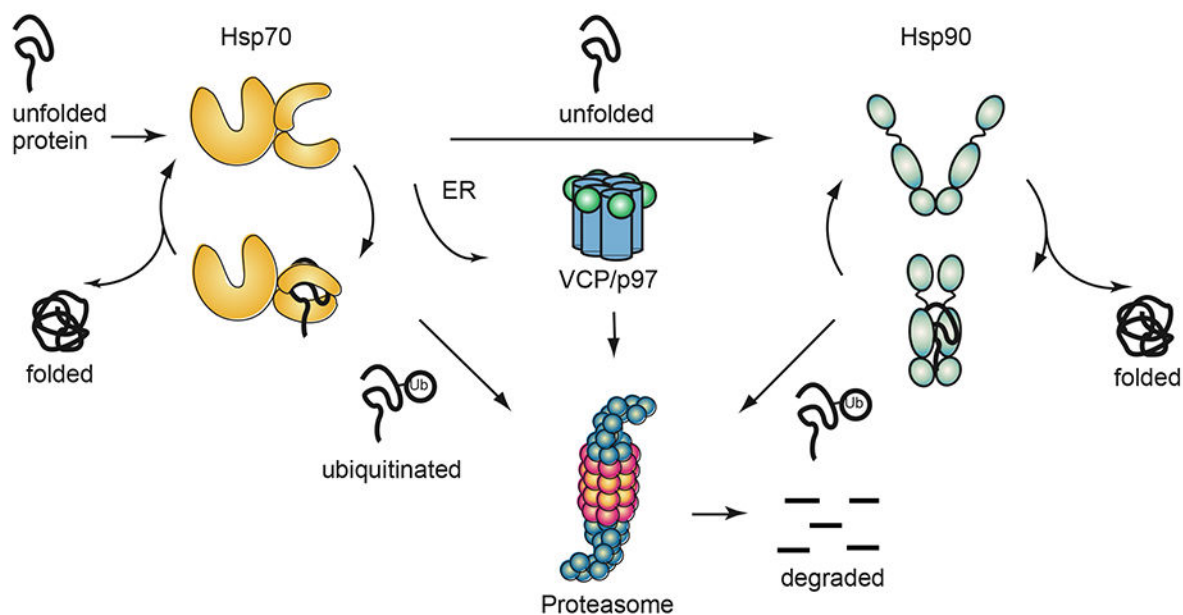
1. Powers ET; Morimoto RI; Dillin A; Kelly JW; Balch WE Biological and chemical approaches to diseases of proteostasis deficiency. *Annu Rev Biochem* 2009, 78, 959–991 [PubMed: 19298183]
2. Voisine C; Pedersen JS; Morimoto RI Chaperone networks: Tipping the balance in protein folding diseases. *Neurobiol Dis* 2010, 40, 12–20 [PubMed: 20472062]
3. Labbadia J; Morimoto RI The biology of proteostasis in aging and disease. *Annu Rev Biochem* 2015, 84, 435–464.4539002 [PubMed: 25784053]
4. Freilich R; Arhar T; Abrams JL; Gestwicki JE Protein-protein interactions in the molecular chaperone network. *Acc Chem Res* 2018, 51, 940–949 [PubMed: 29613769]
5. Liu Y; Ye Y Proteostasis regulation at the endoplasmic reticulum: A new perturbation site for targeted cancer therapy. *Cell Research* 2011, 21, 867–883 [PubMed: 21537343]
6. Whitesell L; Bagatell R; Falsey R The stress response: Implications for the clinical development of hsp90 inhibitors. *Curr Cancer Drug Targets* 2003, 3, 349–358 [PubMed: 14529386]
7. Dai C; Whitesell L; Rogers AB; Lindquist S Heat shock factor 1 is a powerful multifaceted modifier of carcinogenesis. *Cell* 2007, 130, 1005–1018 [PubMed: 17889646]
8. Pakos-Zebrucka K; Koryga I; Mnich K; Ljujic M; Samali A; Gorman AM The integrated stress response. *EMBO Rep* 2016, 17, 1374–1395 [PubMed: 27629041]
9. Joshi S; Wang T; Araujo TLS; Sharma S; Brodsky JL; Chiosis G Adapting to stress - chaperome networks in cancer. *Nature reviews* 2018, 18, 562–575.PMC6108944
10. Workman P; Burrows F; Neckers L; Rosen N Drugging the cancer chaperone hsp90: Combinatorial therapeutic exploitation of oncogene addiction and tumor stress. *Ann N Y Acad Sci* 2007, 1113, 202–216 [PubMed: 17513464]
11. Calderwood SK; Gong J Heat shock proteins promote cancer: It's a protection racket. *Trends Biochem Sci* 2016, 41, 311–323 [PubMed: 26874923]
12. Whitesell L; Lindquist S Inhibiting the transcription factor hsf1 as an anticancer strategy. *Expert Opin Ther Targets* 2009, 13, 469–478 [PubMed: 19335068]
13. Gabai VL; Yaglom JA; Wang Y; Meng L; Shao H; Kim G; Colvin T; Gestwicki J; Sherman MY Anticancer effects of targeting hsp70 in tumor stromal cells. *Cancer Res* 2016, 76, 5926–5932 [PubMed: 27503927]
14. Hadizadeh Esfahani A; Sverchkova A; Saez-Rodriguez J; Schuppert AA; Brehme M A systematic atlas of chaperome deregulation topologies across the human cancer landscape. *PLoS computational biology* 2018, 14, e1005890 [PubMed: 29293508]
15. Rodina A; Wang T; Yan P; Gomes ED; Dunphy MP; Pillarsetty N; Koren J; Gerecitano JF; Taldone T; Zong H; Caldas-Lopes E; Alpaugh M; Corben A; Riolo M; Beattie B; Pressl C; Peter RI; Xu C; Trondl R; Patel HJ; Shimizu F; Bolaender A; Yang C; Panchal P; Farooq MF; Kishinevsky S; Modi S; Lin O; Chu F; Patil S; Erdjument-Bromage H; Zanzonico P; Hudis C; Studer L; Roboz GJ; Cesarman E; Cerchietti L; Levine R; Melnick A; Larson SM; Lewis JS; Guzman ML; Chiosis G The epichaperome is an integrated chaperome network that facilitates tumour survival. *Nature* 2016, 538, 397–401 [PubMed: 27706135]
16. Evans CG; Chang L; Gestwicki JE Heat shock protein 70 (hsp70) as an emerging drug target. *J Med Chem* 2010, 53, 4585–4602 [PubMed: 20334364]

17. Urra H; Dufey E; Avril T; Chevet E; Hetz C Endoplasmic reticulum stress and the hallmarks of cancer. *Trends Cancer* 2016, 2, 252–262 [PubMed: 28741511]
18. Ruan L; Wang Y; Zhang X; Tomaszewski A; McNamara JT; Li R Mitochondria-associated proteostasis. *Annu Rev Biophys* 2020, 49, 41–67 [PubMed: 31928428]
19. Workman P; Powers MV Chaperoning cell death: A critical dual role for hsp90 in small-cell lung cancer. *Nat Chem Biol* 2007, 3, 455–457 [PubMed: 17637775]
20. Dong B; Jaeger AM; Hughes PF; Loiselle DR; Hauck JS; Fu Y; Haystead TA; Huang J; Thiele DJ Targeting therapy-resistant prostate cancer via a direct inhibitor of the human heat shock transcription factor 1. *Science Trans. Med* 2020, 12, eabb5647
21. Mishra SJ; Liu W; Beebe K; Banerjee M; Kent CN; Munthali V; Koren J 3rd; Taylor JA 3rd; Neckers LM; Holzbeierlein J; Blagg BSJ The development of hsp90beta-selective inhibitors to overcome detriments associated with pan-hsp90 inhibition. *J Med Chem* 2021, 64, 1545–1557 [PubMed: 33428418]
22. Anderson DJ; Le Moigne R; Djakovic S; Kumar B; Rice J; Wong S; Wang J; Yao B; Valle E; Kiss von Soly S; Madriaga A; Soriano F; Menon MK; Wu ZY; Kampmann M; Chen Y; Weissman JS; Aftab BT; Yakes FM; Shawver L; Zhou HJ; Wustrow D; Rolfe M Targeting the aaa atpase p97 as an approach to treat cancer through disruption of protein homeostasis. *Cancer Cell* 2015, 28, 653–665 [PubMed: 26555175]
23. Manasanch EE; Orlowski RZ Proteasome inhibitors in cancer therapy. *Nat Rev Clin Oncol* 2017, 14, 417–433 [PubMed: 28117417]
24. Garg G; Khandelwal A; Blagg BS Anticancer inhibitors of hsp90 function: Beyond the usual suspects. *Adv Cancer Res* 2016, 129, 51–88 [PubMed: 26916001]
25. Chatterjee S; Bhattacharya S; Socinski MA; Burns TF Hsp90 inhibitors in lung cancer: Promise still unfulfilled. *Clin Adv Hematol Oncol* 2016, 14, 346–356 [PubMed: 27379696]
26. Goloudina AR; Demidov ON; Garrido C Inhibition of hsp70: A challenging anti-cancer strategy. *Cancer Lett* 2012, 325, 117–124 [PubMed: 22750096]
27. Huang Z; Wu Y; Zhou X; Xu J; Zhu W; Shu Y; Liu P Efficacy of therapy with bortezomib in solid tumors: A review based on 32 clinical trials. *Future Oncology* 2014, 10, 1795–1807 [PubMed: 25303058]
28. Sannino S; Guerriero CJ; Sabnis AJ; Stolz DB; Wallace CT; Wipf P; Watkins SC; Bivona TG; Brodsky JL Compensatory increases of select proteostasis networks after hsp70 inhibition in cancer cells. *J Cell Sci* 2018, 131.PMC6140321
29. Zhu K; Dunner K Jr.; McConkey DJ Proteasome inhibitors activate autophagy as a cytoprotective response in human prostate cancer cells. *Oncogene* 2010, 29, 451–462 [PubMed: 19881538]
30. Sannino S; Yates ME; Schurdak ME; Oesterreich S; Lee AV; Wipf P; Brodsky JL Unique integrated stress response sensors regulate cancer cell susceptibility when hsp70 activity is compromised. *eLife* 2021, 10, e64977 [PubMed: 34180400]
31. Shah SP; Nooka AK; Jaye DL; Bahlis NJ; Lonial S; Boise LH Bortezomib-induced heat shock response protects multiple myeloma cells and is activated by heat shock factor 1 serine 326 phosphorylation. *Oncotarget* 2016, 7, 59727–59741 [PubMed: 27487129]
32. Bai Y; Su X Updates to the drug-resistant mechanism of proteasome inhibitors in multiple myeloma. *Asia Pac J Clin Oncol* 2021, 17, 29–35 [PubMed: 32920949]
33. Powers MV; Clarke PA; Workman P Dual targeting of hsc70 and hsp72 inhibits hsp90 function and induces tumor-specific apoptosis. *Cancer cell* 2008, 14, 250–262 [PubMed: 18772114]
34. Shevtsov M; Multhoff G; Mikhaylova E; Shibata A; Guzhova I; Margulis B Combination of anti-cancer drugs with molecular chaperone inhibitors. *Int J Mol Sci* 2019, 20, 5284
35. Eugenio AIP; Fook-Alves VL; de Oliveira MB; Fernando RC; Zanatta DB; Strauss BE; Silva MRR; Porcionatto MA; Colleoni GWB Proteasome and heat shock protein 70 (hsp70) inhibitors as therapeutic alternative in multiple myeloma. *Oncotarget* 2017, 8, 114698–114709 [PubMed: 29383113]
36. Cavanaugh A; Juengst B; Sheridan K; Danella JF; Williams H Combined inhibition of heat shock proteins 90 and 70 leads to simultaneous degradation of the oncogenic signaling proteins involved in muscle invasive bladder cancer. *Oncotarget* 2015, 6, 39821–39838 [PubMed: 26556859]

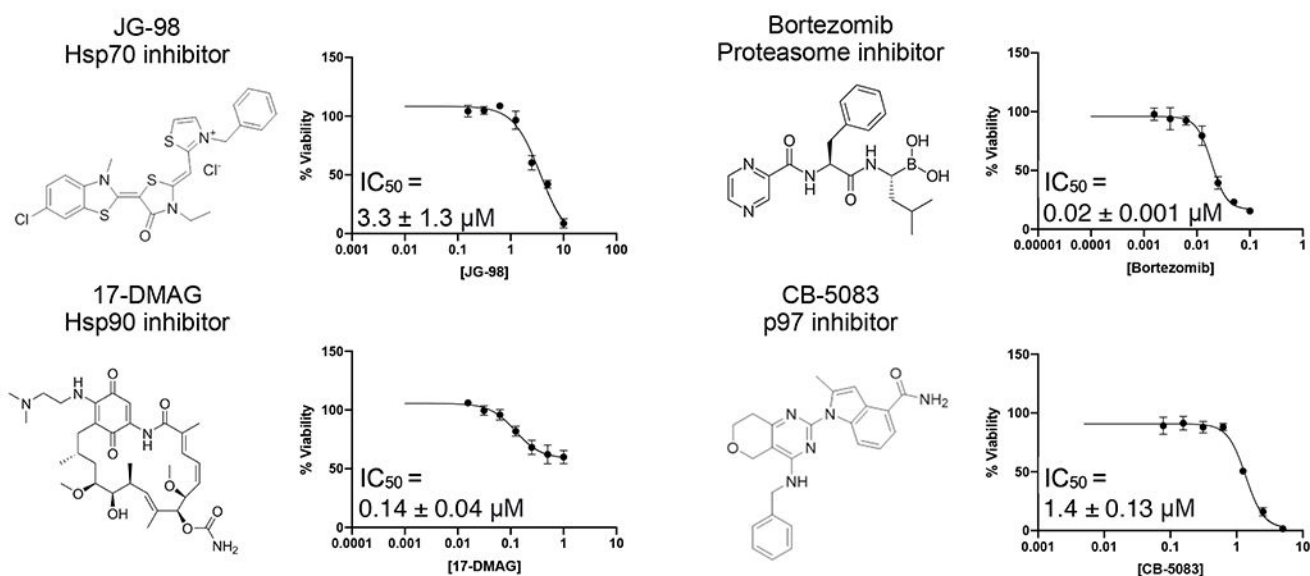
37. Moses MA; Kim YS; Rivera-Marquez GM; Oshima N; Watson MJ; Beebe K; Wells C; Lee S; Zuehlke AD; Shao H; Bingman WE; Kumar V; Malhotra S; Weigel NL; Gestwicki JE; Trepel J; Neckers LM Targeting the hsp40/hsp70 chaperone axis as a novel strategy to treat castration-resistant prostate cancer. *Cancer Res* 2018, 78, 4022–4035 [PubMed: 29764864]
38. Echeverria PC; Picard D Molecular chaperones, essential partners of steroid hormone receptors for activity and mobility. *Biochim Biophys Acta* 2010, 1803, 641–649 [PubMed: 20006655]
39. Hartl FU; Hayer-Hartl M Converging concepts of protein folding in vitro and in vivo. *Nat Struct Mol Biol* 2009, 16, 574–581 [PubMed: 19491934]
40. Vekaria PH; Home T; Weir S; Schoenen FJ; Rao R Targeting p97 to disrupt protein homeostasis in cancer. *Front Oncol* 2016, 6, 181 [PubMed: 27536557]
41. Collins GA; Goldberg AL The logic of the 26s proteasome. *Cell* 2017, 169, 792–806 [PubMed: 28525752]
42. Johnson BD; Schumacher RJ; Ross ED; Toft DO Hop modulates hsp70/hsp90 interactions in protein folding. *J Biol Chem* 1998, 273, 3679–3686 [PubMed: 9452498]
43. Kirschke E; Goswami D; Southworth D; Griffin PR; Agard DA Glucocorticoid receptor function regulated by coordinated action of the hsp90 and hsp70 chaperone cycles. *Cell* 2014, 157, 1685–1697 [PubMed: 24949977]
44. Lemberg MK; Strisovsky K Maintenance of organellar protein homeostasis by er-associated degradation and related mechanisms. *Mol Cell* 2021, 81, 2507–2519 [PubMed: 34107306]
45. Brodsky JL The protective and destructive roles played by molecular chaperones during erad (endoplasmic-reticulum-associated degradation). *Biochem J* 2007, 404, 353–363 [PubMed: 17521290]
46. Petrucelli L; Dickson D; Kehoe K; Taylor J; Snyder H; Grover A; De Lucia M; McGowan E; Lewis J; Prihar G; Kim J; Dillmann WH; Browne SE; Hall A; Voellmy R; Tsuboi Y; Dawson TM; Wolozin B; Hardy J; Hutton M Chip and hsp70 regulate tau ubiquitination, degradation and aggregation. *Hum Mol Genet* 2004, 13, 703–714 [PubMed: 14962978]
47. Dickey CA; Kamal A; Lundgren K; Klosak N; Bailey RM; Dunmore J; Ash P; Shoraka S; Zlatkovic J; Eckman CB; Patterson C; Dickson DW; Nahman NS Jr.; Hutton M; Burrows F; Petrucelli L The high-affinity hsp90-chip complex recognizes and selectively degrades phosphorylated tau client proteins. *J Clin Invest* 2007, 117, 648–658 [PubMed: 17304350]
48. Li X; Srinivasan SR; Connarn J; Ahmad A; Young ZT; Kabza AM; Zuiderweg ER; Sun D; Gestwicki JE Analogs of the allosteric heat shock protein 70 (hsp70) inhibitor, mkt-077, as anti-cancer agents. *ACS medicinal chemistry letters* 2013, 4, 1042–1047
49. Goetz MP; Toft DO; Ames MM; Erlichman C The hsp90 chaperone complex as a novel target for cancer therapy. *Annals Oncology: Official J European Society Medical Oncology / ESMO* 2003, 14, 1169–1176
50. Arkwright R; Pham TM; Zonder JA; Dou QP The preclinical discovery and development of bortezomib for the treatment of mantle cell lymphoma. *Expert Opin Drug Discov* 2017, 12, 225–235 [PubMed: 27917682]
51. Kaul SC; Deocaris CC; Wadhwa R Three faces of mortalin: A housekeeper, guardian and killer. *Exp Gerontol* 2007, 42, 263–274 [PubMed: 17188442]
52. Yadav B; Wennerberg K; Aittokallio T; Tang J Searching for drug synergy in complex dose-response landscapes using an interaction potency model. *Comput Struct Biotechnol J* 2015, 13, 504–513 [PubMed: 26949479]
53. Tallarida RJ Quantitative methods for assessing drug synergism. *Genes Cancer* 2011, 2, 1003–1008 [PubMed: 22737266]
54. Chou TC; Talalay P Quantitative analysis of dose-effect relationships: The combined effects of multiple drugs or enzyme inhibitors. *Adv Enzyme Regul* 1984, 22, 27–55 [PubMed: 6382953]
55. Meyer CT; Wooten DJ; Lopez CF; Quaranta V Charting the fragmented landscape of drug synergy. *Trends Pharm Sci* 2020, 41, 266–280 [PubMed: 32113653]
56. Vlot AHC; Aniceto N; Menden MP; Ulrich-Merzenich G; Bender A Applying synergy metrics to combination screening data: Agreements, disagreements and pitfalls. *Drug Discovery Today* 2019, 24, 2286–2298 [PubMed: 31518641]

57. Feng Q; He B Androgen receptor signaling in the development of castration-resistant prostate cancer. *Front Oncol* 2019, 9, 858 [PubMed: 31552182]
58. Watson PA; Arora VK; Sawyers CL Emerging mechanisms of resistance to androgen receptor inhibitors in prostate cancer. *Nature reviews* 2015, 15, 701–711
59. Eftekharzadeh B; Banduseela VC; Chiesa G; Martinez-Cristobal P; Rauch JN; Nath SR; Schwarz DMC; Shao H; Marin-Argany M; Di Sanza C; Giorgetti E; Yu Z; Pierattelli R; Felli IC; Brun-Heath I; Garcia J; Nebreda AR; Gestwicki JE; Lieberman AP; Salvatella X Hsp70 and hsp40 inhibit an inter-domain interaction necessary for transcriptional activity in the androgen receptor. *Nature Commun* 2019, 10, 3562 [PubMed: 31395886]
60. Ankar J; Sistonen L Regulation of hsf1 function in the heat stress response: Implications in aging and disease. *Annu Rev Biochem* 2011, 80, 1089–1115 [PubMed: 21417720]
61. Wadhwa R; Sugihara T; Yoshida A; Nomura H; Reddel RR; Simpson R; Maruta H; Kaul SC Selective toxicity of mkt-077 to cancer cells is mediated by its binding to the hsp70 family protein mot-2 and reactivation of p53 function. *Cancer Res* 2000, 60, 6818–6821 [PubMed: 11156371]
62. Taipale M; Tucker G; Peng J; Krykbaeva I; Lin ZY; Larsen B; Choi H; Berger B; Gingras AC; Lindquist S A quantitative chaperone interaction network reveals the architecture of cellular protein homeostasis pathways. *Cell* 2014, 158, 434–448 [PubMed: 25036637]
63. Whitesell L; Mimnaugh EG; De Costa B; Myers CE; Neckers LM Inhibition of heat shock protein hsp90-pp60v-src heteroprotein complex formation by benzoquinone ansamycins: Essential role for stress proteins in oncogenic transformation. *Proc Natl Acad Sci U S A* 1994, 91, 8324–8328 [PubMed: 8078881]
64. Hu R; Lu C; Mostaghel EA; Yegnasubramanian S; Gurel M; Tannahill C; Edwards J; Isaacs WB; Nelson PS; Bluemn E; Plymate SR; Luo J Distinct transcriptional programs mediated by the ligand-dependent full-length androgen receptor and its splice variants in castration-resistant prostate cancer. *Cancer Res* 2012, 72, 3457–3462 [PubMed: 22710436]
65. Sannino S; Brodsky JL Targeting protein quality control pathways in breast cancer. *BMC Biol* 2017, 15, 109 [PubMed: 29145850]
66. Richards R; Schwartz HR; Honeywell ME; Stewart MS; Cruz-Gordillo P; Joyce AJ; Landry BD; Lee MJ Drug antagonism and single-agent dominance result from differences in death kinetics. *Nat Chem Biol* 2020, 16, 791–800 [PubMed: 32251407]
67. Srinivasan SR; Cesa LC; Li X; Julien O; Zhuang M; Shao H; Chung J; Maillard I; Wells JA; Duckett CS; Gestwicki JE Heat shock protein 70 (hsp70) suppresses rip1-dependent apoptotic and necroptotic cascades. *Molecular Cancer Res: MCR* 2018, 16, 58–68 [PubMed: 28970360]
68. Ishii T; Seike T; Nakashima T; Juliger S; Maharaj L; Soga S; Akinaga S; Cavenagh J; Joel S; Shiotsu Y Anti-tumor activity against multiple myeloma by combination of kw-2478, an hsp90 inhibitor, with bortezomib. *Blood Cancer J* 2012, 2, e68 [PubMed: 22829970]
69. Richardson PG; Mitsiades CS; Laubach JP; Lonial S; Chanan-Khan AA; Anderson KC Inhibition of heat shock protein 90 (hsp90) as a therapeutic strategy for the treatment of myeloma and other cancers. *British J Haematol* 2011, 152, 367–379
70. Cavenagh J; Oakervee H; Baetiong-Caguioa P; Davies F; Gharibo M; Rabin N; Kurman M; Novak B; Shiraishi N; Nakashima D; Akinaga S; Yong K A phase i/ii study of kw-2478, an hsp90 inhibitor, in combination with bortezomib in patients with relapsed/refractory multiple myeloma. *Br J Cancer* 2017, 117, 1295–1302 [PubMed: 28873084]
71. Dhama K; Latheef SK; Dadar M; Samad HA; Munjal A; Khandia R; Karthik K; Tiwari R; Yattoo MI; Bhatt P; Chakraborty S; Singh KP; Iqbal HMN; Chaicumpa W; Joshi SK Biomarkers in stress related diseases/disorders: Diagnostic, prognostic, and therapeutic values. *Frontiers Molec Biosci* 2019, 6, 91
72. Bagatell R; Paine-Murrieta GD; Taylor CW; Pulcini EJ; Akinaga S; Benjamin IJ; Whitesell L Induction of a heat shock factor 1-dependent stress response alters the cytotoxic activity of hsp90-binding agents. *Clin Cancer Res* 2000, 6, 3312–3318 [PubMed: 10955818]
73. Tiligada E Chemotherapy: Induction of stress responses. *Endocrine-Related Cancer* 2006, 13 Suppl 1, S115–124 [PubMed: 17259552]
74. Kim W; Lee S; Seo D; Kim D; Kim K; Kim E; Kang J; Seong KM; Youn H; Youn B Cellular stress responses in radiotherapy. *Cells* 2019, 8, 1105

## A. Schematic of major nodes of proteostasis network



## B. Chemical structures and dose-response of proteostasis inhibitors in 22Rv1 cells

**Figure 1.**

Proteostasis inhibitors, targeting multiple nodes of the proteostasis network, have anti-proliferative effects in 22Rv1 prostate cancer cells. A. A subset of the proteostasis network is shown, highlighting the connections between the major nodes: Hsp70, Hsp90, p97, and the proteasome. Together, these factors guide protein folding and turnover, working together to mediate client “hand-off”. B. Inhibitors of proteostasis nodes limit growth of 22Rv1 cells. In this study, four inhibitors were used: JG-98 (Hsp70 inhibitor), 17-DMAG (Hsp90 inhibitor), bortezomib (proteasome inhibitor) and CB-5083 (p97 inhibitor). Cells

were incubated with the indicated compound for 72 hours, and viability measured via Cell Titer Glo (see Methods). Results are the average of experiments performed in quadruplicate and the error bars represent SD. Some error bars are smaller than symbols.

Author Manuscript

Author Manuscript

Author Manuscript

Author Manuscript

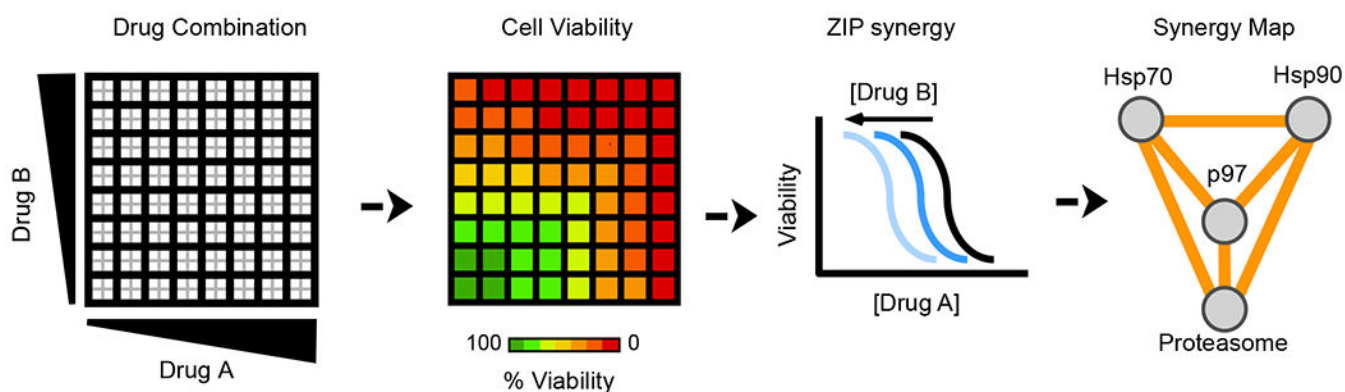


**Figure 2.**

Workflow for the measurement of additivity, synergy or antagonism amongst proteostasis inhibitors. Briefly, cells are aliquoted to 384-well plates and allowed to adhere for one day. Then, two drugs (A and B) are added in an 8x8 matrix format, with 7 doses per compound, using 2-fold dilutions (see Methods for tested concentrations) and a DMSO solvent control. Treatments were performed in quadruplicate, with 4 wells per each dose combination (grey squares). After 72-hours of treatment, cell viability was measured using Cell Titer Glo, and synergy determined through the ZIP synergy model. Drug-combination screens were performed twice per cell line, and ZIP synergy score was averaged between replicates. Under this model, addition of Drug B reducing the potency of Drug A (blue lines) would be considered synergy. ZIP scores around zero (between 1.5 and -1.5) were considered additive, while scores above 1.5 were considered synergistic and those below -1.5 were considered antagonistic. To map these relationships onto the proteostasis subnetwork (see Fig 1A), we plotted the nodes and created lines between them to indicate whether the ZIP synergy score was additive, synergistic or antagonistic for each tested cell line (termed a Synergy Map).

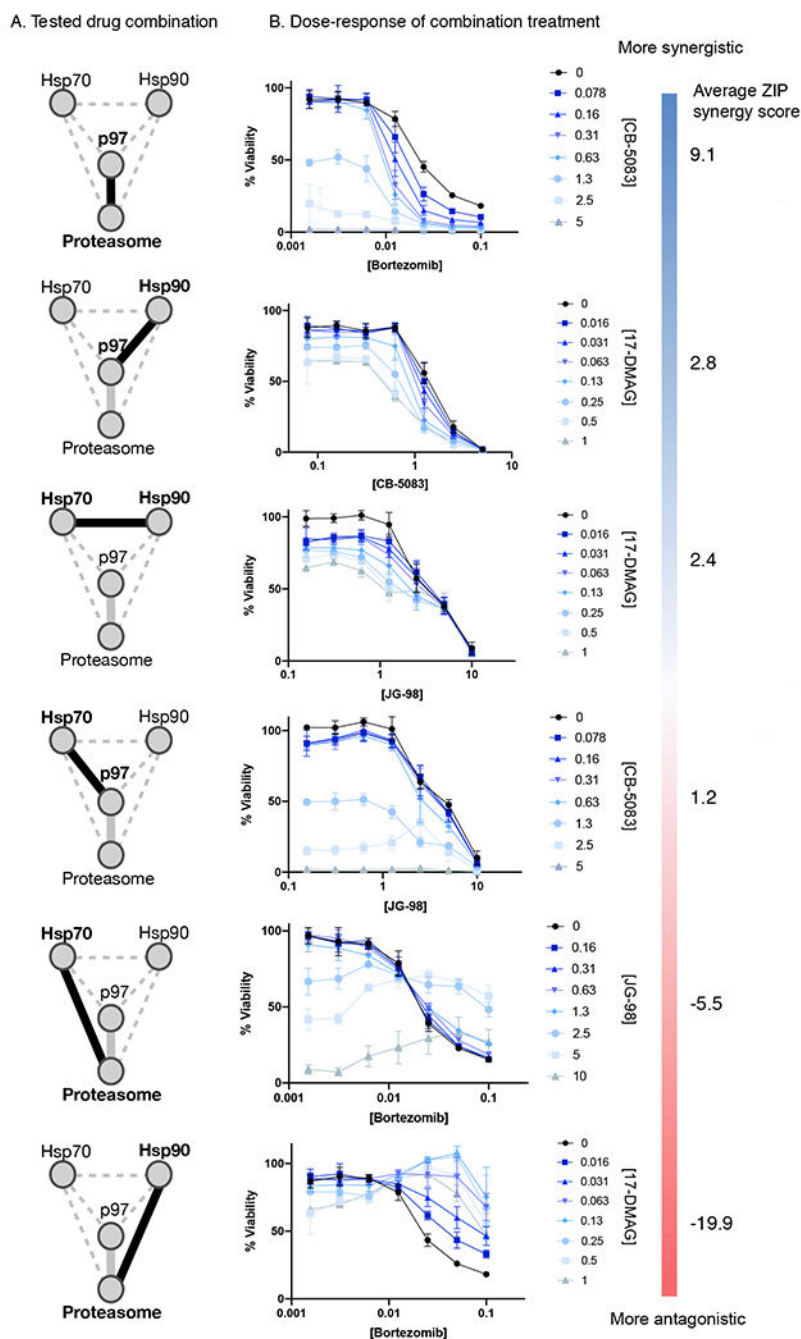


**Figure 3.**

Combinations were either additive, synergistic or antagonistic in 22Rv1 cells. A. For each combination, a black line and bolded text indicates the tested nodes on the Synergy Map in the highlighted adjacent dose-response panel. B. Dose-response curves from each combination are used to highlight additivity, synergy or antagonism. In each graph, the single-agent (black) and combination treatments (blue curves) are shown. Curves are arranged from top to bottom from the most synergistic to the most antagonistic, with the

average ZIP synergy scores shown. For the full matrix landscape of the cell viability and synergy results, see Figure S1. All concentrations are in micromolar.

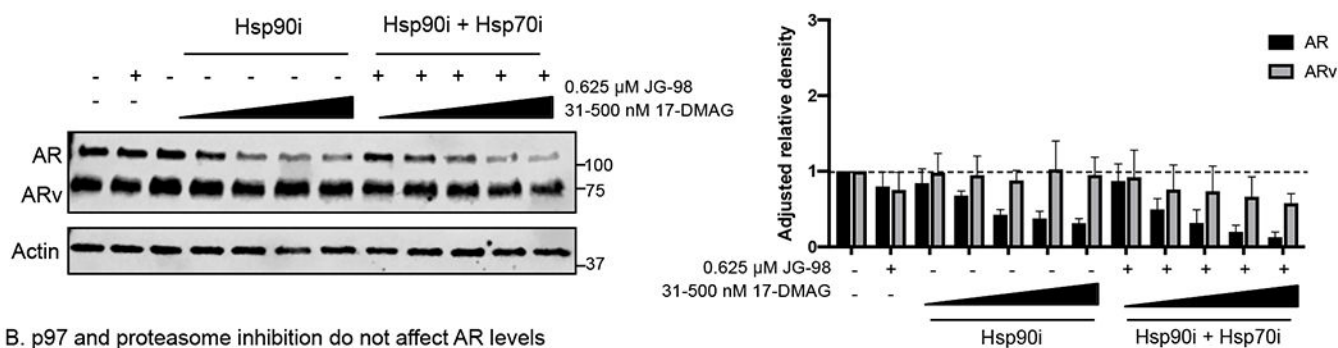
Author Manuscript

Author Manuscript

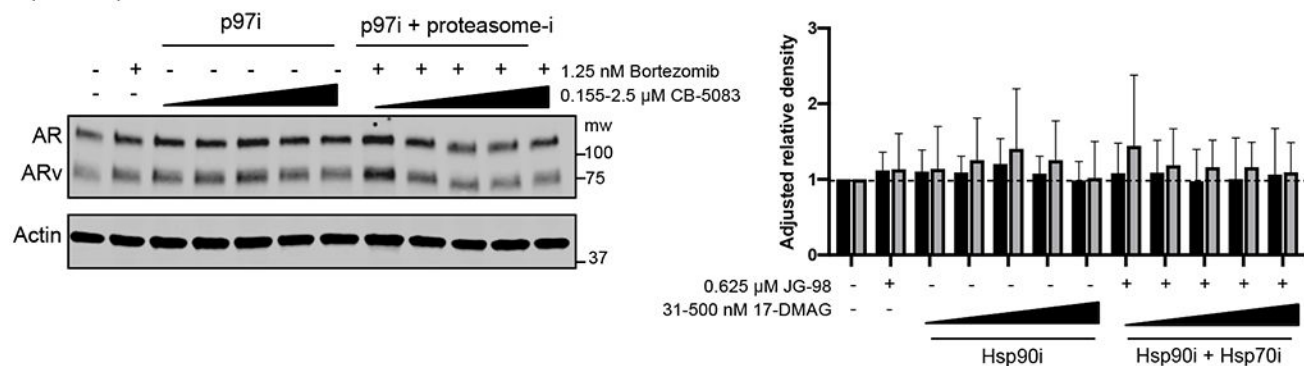
Author Manuscript

Author Manuscript

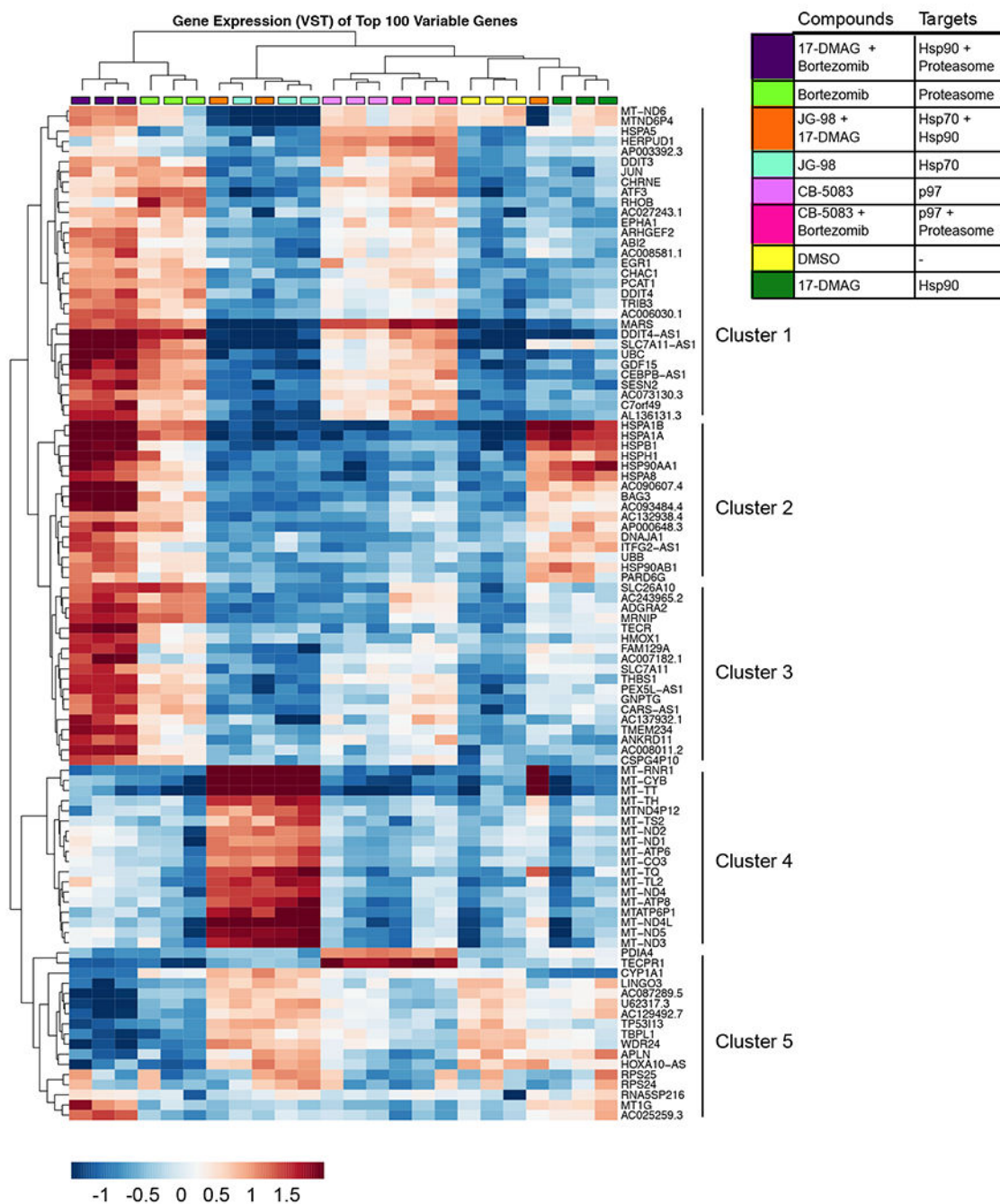
## A. Hsp70 and Hsp90 inhibition reduce AR levels



## B. p97 and proteasome inhibition do not affect AR levels

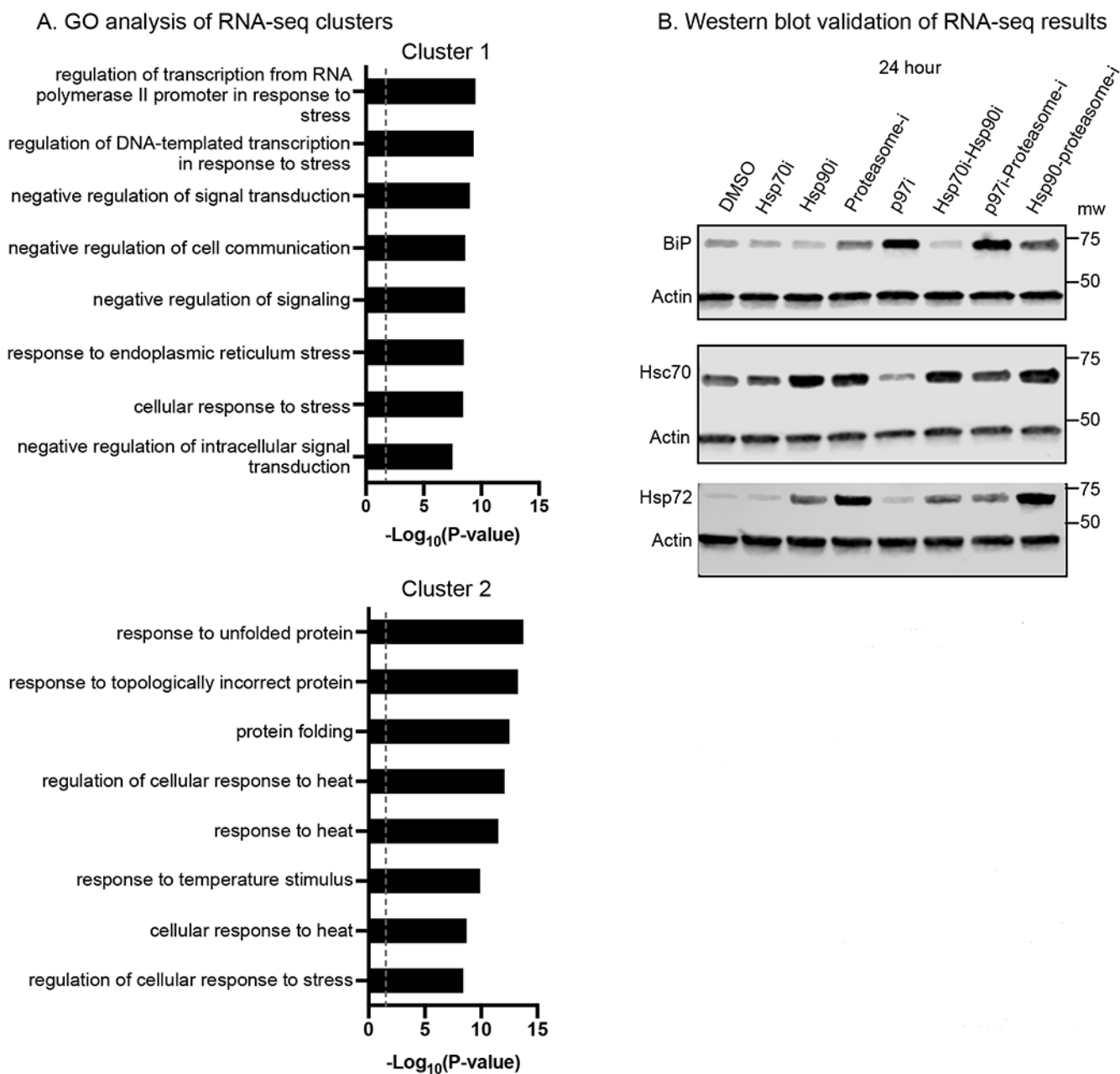
**Figure 4.**

Some combinations reduce androgen receptor levels, but others do not. Effects of proteostasis inhibitor combinations on AR levels in 22Rv1 cells following 6-hour treatment. A. Treatment with the Hsp90 inhibitor 17-DMAG reduces the levels of full length AR, and Hsp70 inhibitor JG-98 treatment reduces levels of both AR and ARv in 22Rv1 cells after 6 hours. The combination was effective at reducing both proteins. B. Neither the p97 nor proteasome inhibitor, or their combination, had an effect on AR or ARv levels at 6 hours. Western blots are representative of experiments performed in triplicate. The blots were quantified in NIH Image J and the average density adjusted to the loading control and DMSO treatment was plotted on the right. Error bars represent SD.



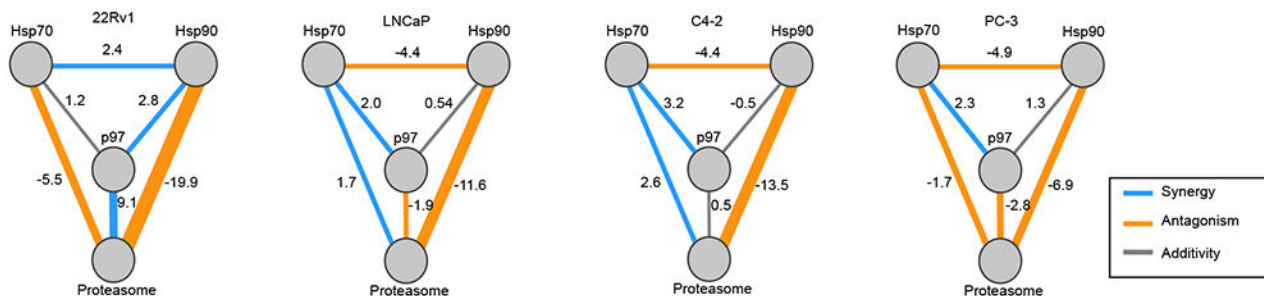
**Figure 5.**

RNA-seq data highlights differences in gene expression following single-agent and combination proteostasis inhibitor treatment. 22Rv1 cells were treated with indicated compounds for 6 hours, after which RNA-seq was performed (see Methods). The top 100 variably expressed genes across all conditions were clustered and further analyzed.

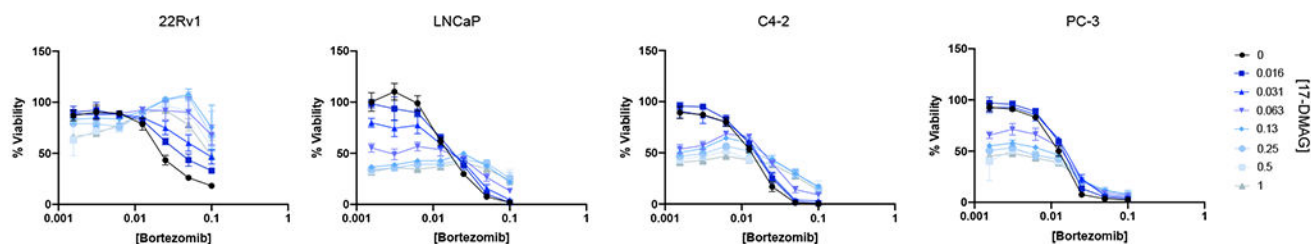
**Figure 6.**

RNA-seq studies and protein level validation highlight differences in activation of stress response pathways between single-agent and combination proteostasis inhibitor treatments. A. Gene ontology (GO) analysis of clusters 1 and 2 from top variably expressed genes (see Figure 5). Top 8 most significantly enriched GO terms are shown. B. BiP, Hsc70, and Hsp72 levels were probed via Western blot following 24 hours of compound treatment (see Methods for concentrations used). Protein levels at 24 hours closely match transcriptomic data and are differentially expressed across single-agent and combination proteostasis inhibition. Results are representative of experiments performed in triplicate.

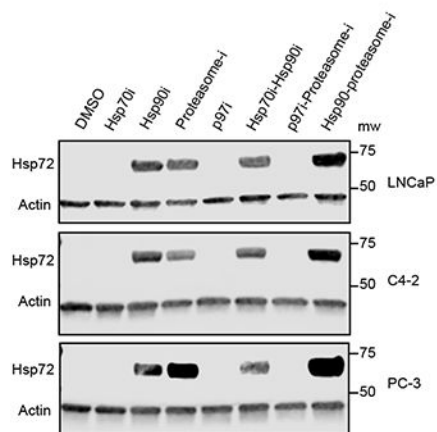
## A. Synergy maps of proteostasis inhibitors across prostate cancer



## B. Hsp90-Proteasome inhibition is antagonistic across all four cell lines



## C. Hsp72 is especially upregulated following Hsp90-proteasome inhibition

**Figure 7.**

Expanded screens in additional prostate cancer cell lines reveals both similarities and differences in their responses to combinations of proteostasis inhibitor treatment. A. Synergy maps depicting the relationship between proteostasis nodes from the drug-combination screens. Synergy is blue, antagonism is orange, and additivity is gray. Cutoffs defined in Figure 2 were applied here. Screens were performed as described in Figure 2, with each dose-combination performed in quadruplicate. Each screen was performed twice per cell line, and synergy scores were averaged. B. Representative dose-response curves from the antagonistic combination of proteasome-Hsp90 inhibitors. In each example, the proteasome inhibitor (bortezomib) alone is shown in black, while the combinations with the Hsp90 inhibitor 17-DMAG are shown with blue lines. Results are the average of quadruplicate and error bars are SD. Some error bars are smaller than the symbols. C. Hsp72 is upregulated following Hsp90 and proteasome inhibition in all of the cell lines tested, by Western blot.

Results are representative of experiments performed in triplicate. See Methods for the concentrations used.

Author Manuscript

Author Manuscript

Author Manuscript

Author Manuscript